Electromigration Effect on Intermetallic Growth and Young's Modulus in SAC Solder Joint

LUHUA XU,[1] JOHN H.L. PANG,[1,3] FEI REN,[2] and K.N. TU[2]

1.—School of Mechanical & Production Engineering, Nanyang Technological University, Singapore 639798. 2.—Department of Materials Science and Engineering, University of California, Los Angeles, CA 90095-1595. 3.—E-Mail: mhlpang@ntu.edu.sg

Solid-state intermetallic compound (IMC) growth behavior plays an important role in solder joint reliability of electronic packaging assemblies. The directional impact of electromigration (EM) on the growth of interfacial IMCs in Ni/SAC/Ni, Cu/SAC/Ni single BGA ball solder joint, and fine pitch ball-grid-array (FPBGA) at the anode and cathode sides is reported in this study. When the solder joint was subjected to a current density of 5,000 A/cm^2 at 125°C or 150°C, IMC layer growth on the anode interface was faster than that on the cathode interface, and both were faster than isothermal aging due to the Joule heating effect. The EM affects the IMC growth rate, as well as the composition and mechanical properties. The Young's modulus and hardness were measured by the nanoindentation continuous stiffness measurement (CSM) from planar IMC surfaces after EM exposure. Different values were observed at the anode and cathode. The energy-dispersive x-ray (EDX) line scan analysis was conducted at the interface from the cathode to anode to study the presence of species; Ni was found in the anode IMC at SAC/Cu in the Ni/SAC/Cu joint, but not detected when the current was reverse. Electron-probe microanalysis (EPMA) measurement on the Ni/SAC/Ni specimen also confirmed the polarized Ni and Cu distributions in cathode and anode IMCs, which were $(Ni_{0.57}Cu_{0.43})_3Sn_4$ and $(Cu_{0.73}Ni_{0.27})_6Sn_5$, respectively. Thus, the Young's moduli of the IMC are 141 and 175 GPa, respectively.

Key words: Electromigration, lead-free SnAgCu solder, intermetallic compound, nanoindentation

INTRODUCTION

Lead-free solders will replace tin-lead solders due to legislation to replace lead (Pb) in electronic solders from July 1, 2006. The electronic packaging industry is preparing for Pb-free soldering manufacturing of electronics assemblies.[1,2] At the same time, the size of the solder joint becomes smaller and smaller, with the solder sphere diameter going down to 100 μm. This is expected to reduce to 50 μm and below in the future. Electromigration (EM) due to high current density has become a serious concern for packaging reliability.[3] The phenomenon of EM has been the subject of intense study. Both theoretical and experimental work has been reported.[4–10] High current density in the integrated circuit interconnects causes a net metallic atoms flux. The atoms generally migrate in the same direction as the electron flow. This leads to a continuous impact and causes the atoms to pile up in the direction of the electron flow (anode) and produces voids in an upstream direction (cathode) with respect to the electron flow. These defects are the most persistent and serious reliability failures in integrated circuits.[5] In solder joints, the distribution of current density is far from uniform. The current density can be about one to two orders of magnitude larger than average at the joint corner, which means 10^5 A/cm^2. Voids can form and expand quickly at corners. With the voids or crack growth, the nonuniformity of the current density over the solder joint increases. Because the Joule heating is proportional to the square of the current density, the local temperature is much higher than average.[9] The current crowding effect therefore plays a double role here: both the elevated local current density and temperature accelerate the intermetallic compound (IMC) growth. The impact of EM on SnPb and Pb-free solder joint was reported in previous studies;[5–7] the solder undergoes dramatic changes. In SnPb solder, the very fine

(Received March 10, 2006; accepted June 30, 2006)

grained two-phase system experiences phase coalesce and segregation. One of the major concerns for both SnPb and Pb-free solder joint is the directional effect of IMC growth at the anode and IMC dissolution/voiding at the cathode. The EM drives atoms from cathode to anode. Therefore, it tends to dissolve or retard the growth IMC at the cathode but build up or enhance the growth IMC at the anode. The solid-state dissolution of the under-bump metallurgy (UBM) due to EM at the cathode will be a reliability issue. The polarity effect of IMC growth rate on different UBM and SnPb solder was reported.

In this study, the impact of EM on the IMC growth on SnAgCu with different UBM couples, e.g., Ni/SAC/Ni, Cu/SAC/Ni, and Cu/SAC/Cu, is tested on a single ball-grid-array (BGA) ball specimen and fine pitch ball-grid-array (FPBGA) specimen. The IMC growth rate as well as the IMC composition was studied. The mechanical properties of the IMC at the anode and cathode were measured by nanoindentation CSM from the planer IMC surface rather than the cross-sectioned interface.[11] The energy-dispersive x-ray (EDX) line scan analysis was conducted at the interface from the anode to cathode.

EXPERIMENTAL PROCEDURES

The single BGA ball solder joint specimen consists of a single 95.5Sn-3.8Ag-0.7Cu solder (SAC) ball with diameter of 0.5 mm, soldered between two pieces of FR4 substrate with copper pad opening of 0.3 mm, as shown in Fig. 1. The fabrication of the specimen was reported in our earlier studies.[12] The Ni/Au surface finish on copper pad has a nickel (Ni) layer thickness of 5 μm and a gold (Au) flash thickness of 0.05 μm. The copper pad thickness is 30 μm. The FR4 substrate has dimensions of 12 mm $\times$ 3 mm $\times$ 0.5 mm. The specimens were prepared using an eight-zone reflow oven. The solder reflow profile with a peak temperature of 250°C and time above melting point of 120 sec was used in the fabrication. Further study was conducted on the FPBGA 324 I/O specimen, a daisy chain was designed to connect all the solder balls in series, by which thermal cycling and an isothermal aging study were conducted in previous studies.[12] A slice of BGA solder balls was cut from the entire assembly to conduct the EM test, as shown in Fig. 2. The advantage of using slice specimen rather than the entire assembly is to avoid the possible early failure among any one solder joint in 324 joints. It was also noted that heat dissipation for slice specimen is better than using the entire assembly.

The EM test was performed on the solder joint specimen in a thermal chamber with ambient temperature of 125°C or 150°C. To observe the effect of Joule heating, in-situ temperature measurement was conducted on a cross-sectioned slice FPBGA specimen when the sample was subjected to EM exposure. An infrared thermal imaging system was used to determine the two-dimensional temperature distribution in solder joint interconnects. For the EM test, the two enameled wires were connected to pass a constant current, generating a nominal average current density of 5×10^3–1×10^4 A/cm^2; calculation of current density is based on the area of the pad. The test time ranged from 1–10 days with a tracking accuracy of 30 min. Isothermal aging for the specimen at the same ambient temperature was conducted for comparison. Upon completion of the aging treatment, the specimens were cross-sectioned for characterization using a JEOL JSM-5410LV scanning electron microscope under an accelerated voltage of 20 kV. For investigation of the IMC layer at the anode and cathode, digital imaging techniques were employed in the measurement of the average IMC growth thickness. Two polylines R1 and R2 were created manually along the edge of the IMC by using the tracing tool. Then, the average distance between the two polylines was calculated automatically. Line scan composition analysis using EDX was conducted to characterize the composition distribution from anode to cathode in terms of the EM test. Quantitative composition analysis using electron-probe microanalysis (EPMA) was conducted on the ENIG/SAC/ENIG specimen after EM.

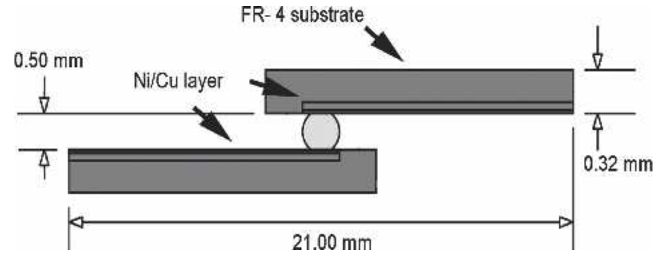

Fig. 1. Single SAC387 solder sphere joint specimen with two FR-4 substrates; the metallization is Ni on copper. The diameter of solder ball: 0.5 mm; and pad opening: 0.3 mm.

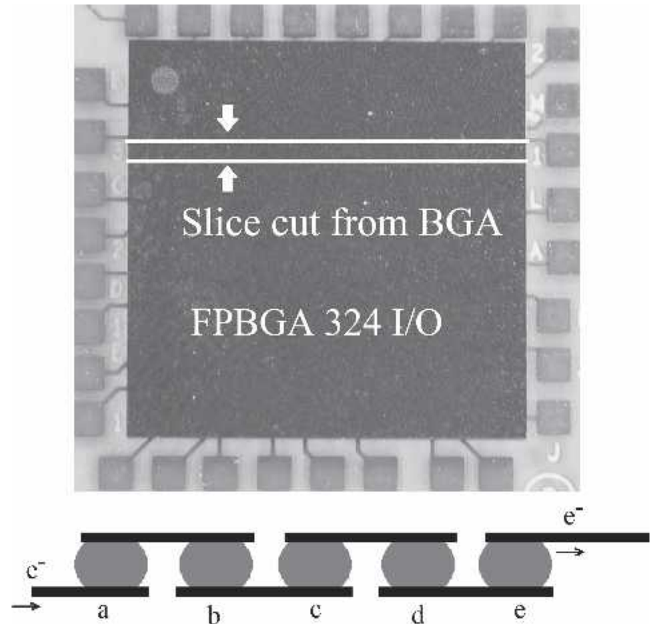

Fig. 2. FPBGA component with 324 I/Os and a slice with five solder balls cut from the component for applying current.

Nanoindentation CSM tests on IMC layers were performed using an instrumented system MTS indentation XP with a Berkovich diamond pyramid tip. The measurement is conducted from the planar IMC surface and the solder joint specimens were selectively etched using 13 vol.% nitric acid, which removed the SAC solder and exposed the IMC interfaces. The IMC surface was then slightly polished by the alumina suspensions until a flat IMC surface was obtained. The indentation test was conducted on these flat surfaces for the specimens before and after the EM test. The CSM standard hardness and modulus test program was used with a depth limit into a surface of 300–400 nm. The CSM harmonic depth and the harmonic frequency were 2 nm and 45 Hz, respectively. The major difference between the CSM technique and conventional method is the method of finding the contact stiffness.[13,14] For conventional nanoindentation, stiffness is the differentiation of load over penetration at the maximum depth of the unloading curve. For CSM, stiffness is measured continuously by the harmonic oscillating force and the displacement response added to the nominally increasing load. The hardness and modulus of IMCs reported in this study were the average value when displacement into the surface increased from 100 nm to 300 nm. For each specimen, at least 7–10 points were tested.

RESULTS AND DISCUSSION

Joule Heating Characterization

Joule heating effect and current crowding accelerate the effect of EM in solder joints. It is necessary to measure the local temperature at the solder joint during the accelerated EM test as temperature could be much higher than ambience. Figure 3

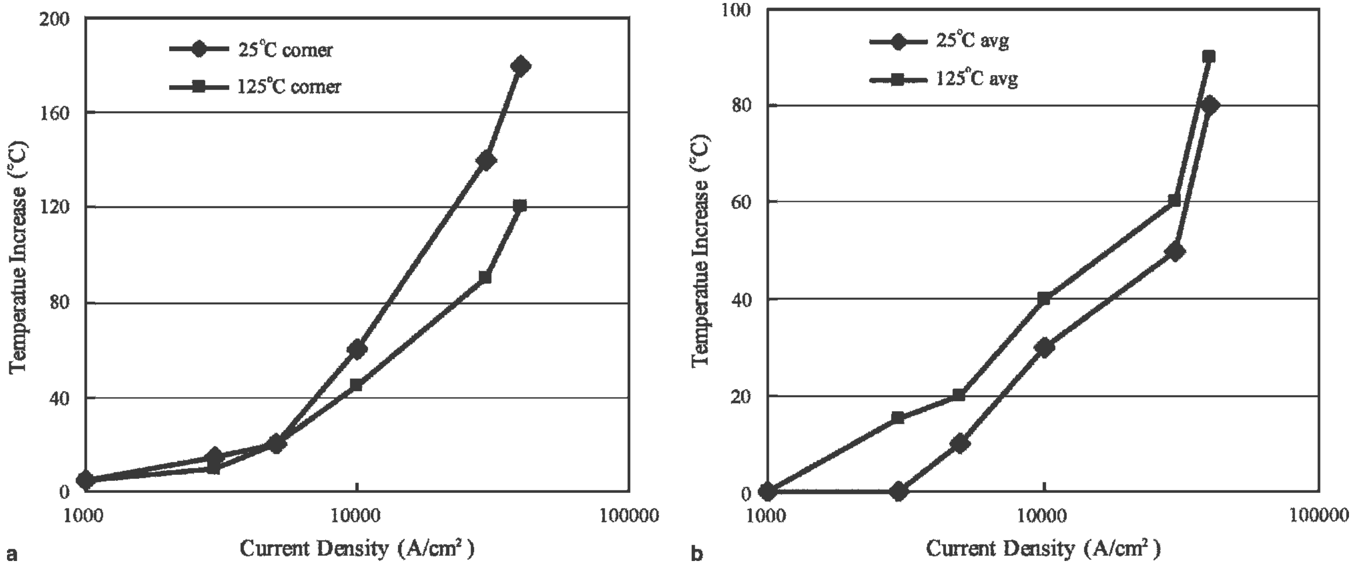

Fig. 3. Temperature increase versus current density at (a) corner and (b) center, which was measured by an infrared thermal imaging system.

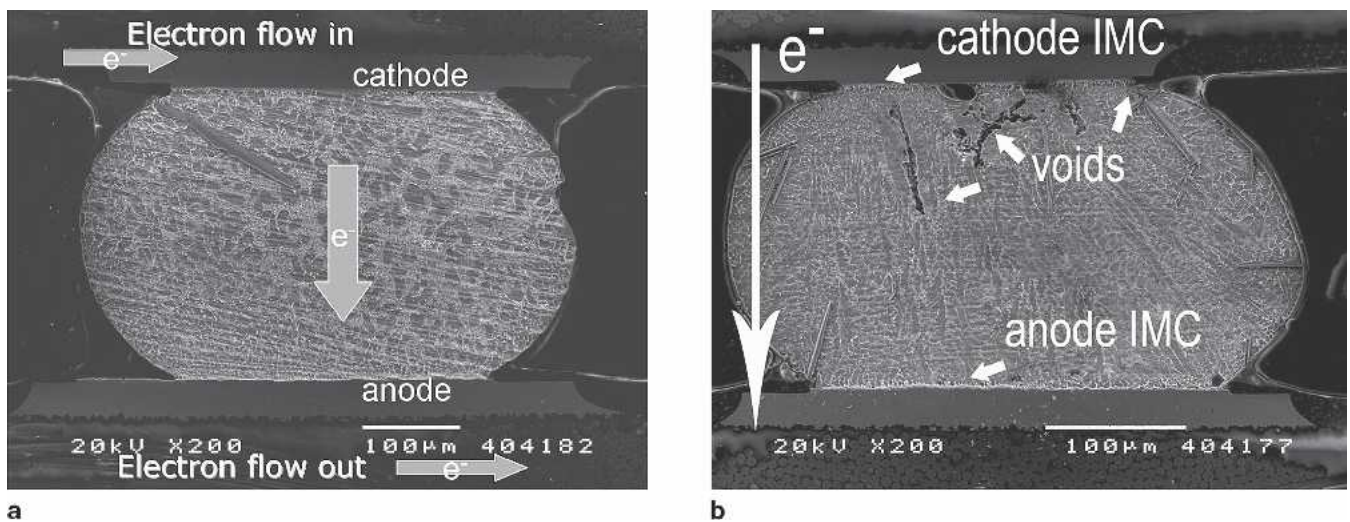

Fig. 4. Representative solder ball microstructure before and after the EM test: (a) 0 h and (b) 260 h; the direction of the electron flow and the corresponding effect are shown.

shows the temperature versus current density at the cross-sectioned slice solder joint measured by the infrared thermal imaging system. The chamber background was set at room temperature (25°C) or 125°C. The temperature increase was observed on the solder joint and compared to the ambient. The temperature increase at 125°C is higher than that at room temperature, which is reasonable because the resistance coefficient for SAC is higher at higher temperature, and the heat generated is greater than at room temperature. For current density below 10^4 A/cm^2 in this study, joule heating only caused a temperature increment of 10–30°C. It is noted that the temperature increase for this specimen could reach 180°C when the current density is about 4×10^4 A/cm^2 (solder was molten when ambient is 125°C). Thus, higher current density studies were not conducted on this specimen.

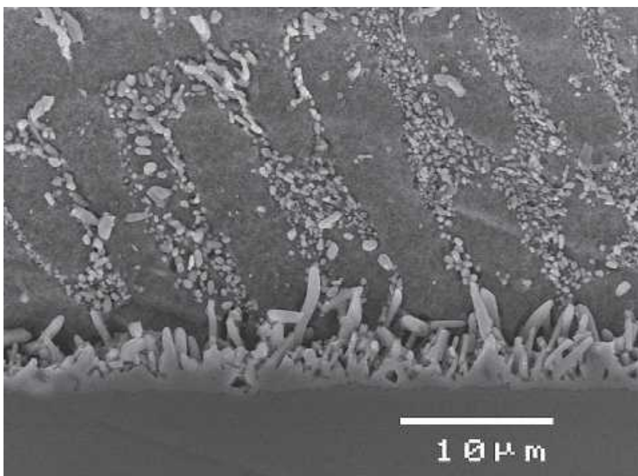

Fig. 5. SEM image of IMC morphology for the as-reflowed specimen without EM exposure, SAC/Ni; the IMC is needlelike.

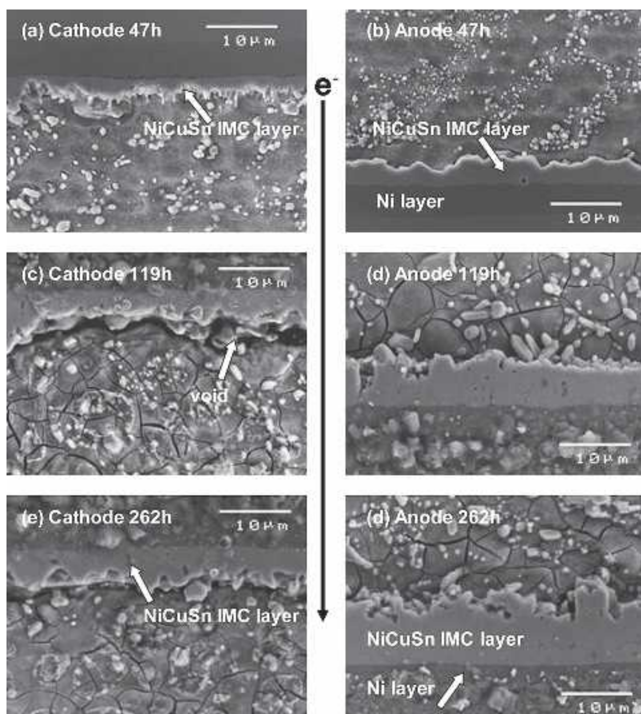

Fig. 6. Interfacial IMC morphology revolution subject to EM at $5{\cdot}10^3$A/cm^2 up to 262 h; the dramatic changes at anode and cathode of SAC/Ni are presented.

The EM Effect on IMC Thickening

The cross section of the Ni/SAC/Ni single solder joint specimen before and after EM is shown in Fig. 4a and b; the direction of electron flow is as indicated, with current density of 5,000 A/cm^2 at 150°C up to 10 days. During the EM exposure, thermal and EM effect interact at the interface. However, the interactions at the cathode and the anode are different due to the directional EM effect. At the cathode, the electron flow is from the IMC to solder, while at the anode, the flow direction is reversed. Thus, EM enhances the IMC formation at the anode and causes IMC dissolution at the cathode. Figure 4a shows the as-reflowed solder joint, in which the cross-sectioned interface was slightly etched after being fine polished with 0.05 gamma alumina. The microstructure of the solder joint after reflow is typically globular Sn-rich phases surrounded by small Ag_3Sn phases, and Cu_6Sn_5 also presents. Some large Ag_3Sn IMC rods are formed in the solder and can be as long as 100 μm or more.[12] Figure 4b

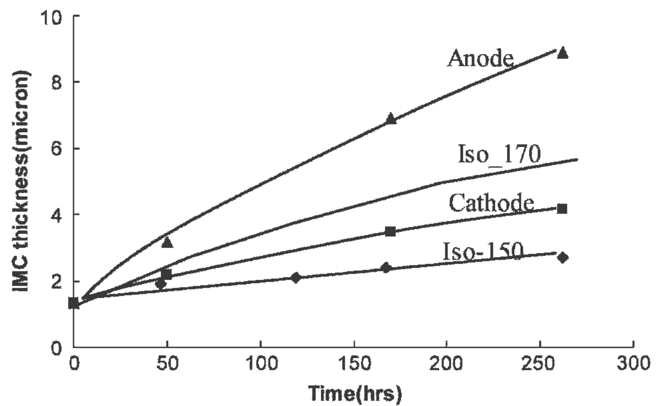

Fig. 7. Electromigration effect on IMC growth: (▲) anode, electron Sn → Ni; (■) cathode, electron Ni → Sn; and (◆) isothermal at 150°C and calculated curve isothermal at 170°C.

Table I. Diffusion Coefficients of the Solder Joint with/without EM, for Ni/SAC/Ni Single Solder Sphere Joint Subject to Current to 5,000 A/cm^2, Ambient Temperature of 150°C

Symbol	Definition of Coefficient	Value at 170°C with Current Density of 5 kA/cm^2
Di	Isothermal diffusivity	0.3208
Dc	Cathode diffusivity	0.1754
Da	Anode diffusivity	0.472
Di-Dc	Dissolution	0.1454
Da-Di	Elevatory coefficient	0.1512

shows the cross-sectioned morphology after EM exposure for 262 h; voids near the IMC layer and solder at the cathode side were observed. Some irregular voids exist in the solder bump, as indicated by the arrow. They must have formed during the EM exposure because pre-existing gassing voids are normally spherical in shape, due to the surface tension in molten solder/vapor interface. Hillocks at the anode side were not seen in Fig. 4b, because the specimen was cross-sectioned after the EM test, and the polished surface is flat.

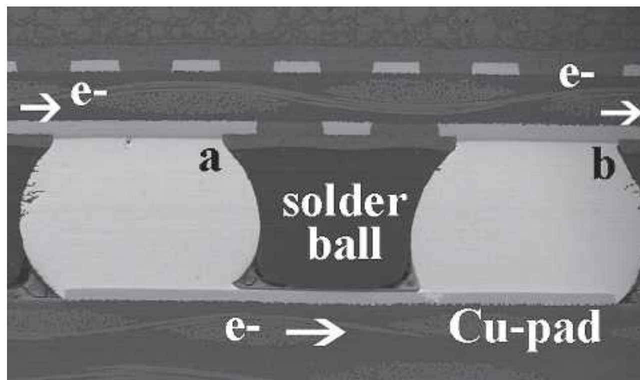

Fig. 8. Cross-sectioned FPBGA solder joint, showing the direction of the electron flux through the two daisy chained solder balls with the EM test at 5,000 A/cm^2; the directional effect of current at solder ball a and b is inverse.

Figure 5 shows the interfacial morphology without EM exposure; the IMCs on the solder/nickel interface are irregular and grow in a needlelike manner. The IMC layers at both sides are identical. The NiCuSn ternary IMC growth at the cathode and anode sides with different aging times was observed. Figure 6 shows the SEM images after EM exposure up to 260 h at 150°C with current density of 5,000 A/cm^2. This shows that EM caused the different IMC growth rate at the anode and cathode sides. The growth rate of NiCuSn ternary IMC at the anode is much faster than that at the cathode side. After 49 h of EM exposure, as shown in Fig. 6a and b, both cathode and anode IMCs become layerlike. Coalescence of the IMC needles leads to lateral thickening and ripening. The IMC thickness at the anode is larger than that at the cathode. The difference of thickness increases as the current is continuously applied to the sample. Some interfacial voids could be seen at the cathode side, as shown in Fig. 6c. Finally, after 262 h of EM

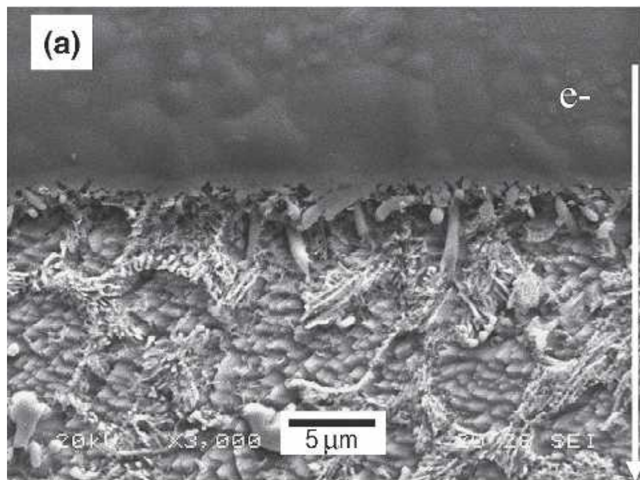

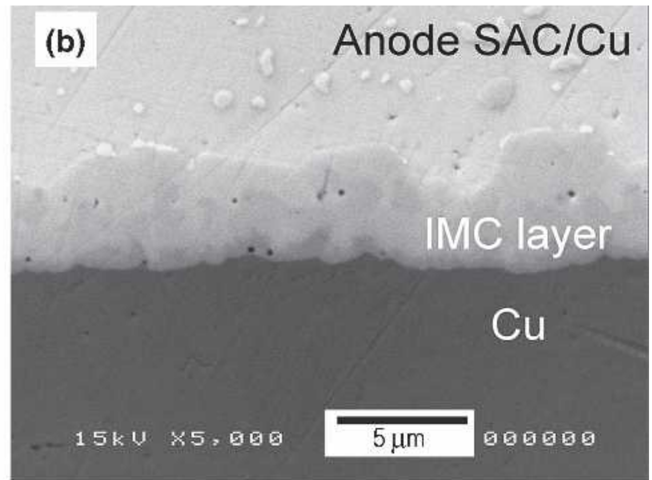

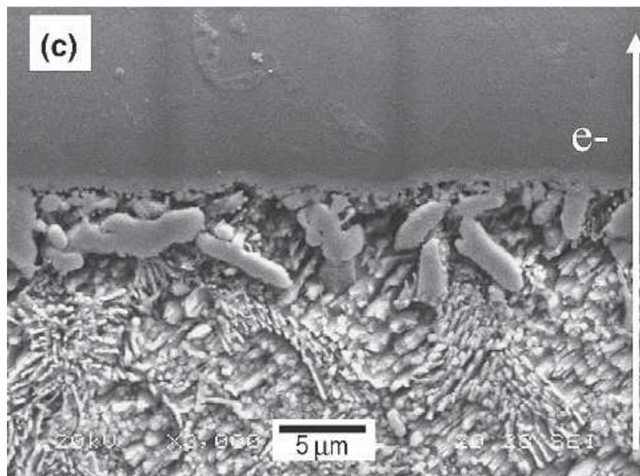

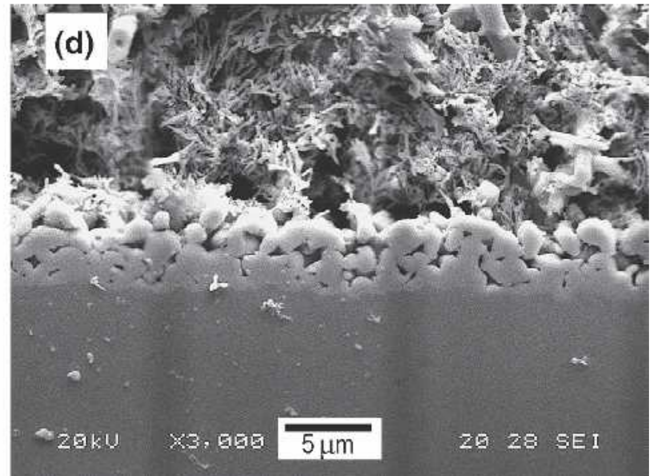

Fig. 9. IMC growth at Ni/SAC/Cu-OSP solder joint, take Fig. 8 as reference. Solder ball a: (a) Ni/SAC, cathode (b) SAC/Cu anode; solder ball b: (c) Ni/SAC anode (d) SAC/Cu cathode.

test aging, the IMC thickness at the anode increased to about 9 μm, while the Ni layer is almost completely consumed. At the cathode side, the IMC thickness is about 5 μm. However, the IMC layer thickness at the cathode is not uniform because voids form at some locations and thus the IMC growth stops there.

The IMC thicknesses at the anode and cathode were measured using digital imaging software; the result is compared with the IMC growth without current at 150°C, as shown in Fig. 7. It is interesting to see that the IMC thickness at both the anode and cathode sides grows faster than in isothermal aging. Theoretically, the IMC growth on the cathode was supposed to be lower than isothermal aging at the same temperature because EM enhances the IMC dissolution at the cathode. However, considering the joule heating effect on the solder joint, it is noted that the actual temperature on the solder joint is higher than ambient temperature. The joule heating effect should be removed in order to merely consider the effect of atomic flux caused by EM. From Fig. 3, it can be seen that the temperature increase at 150°C and 5,000 A/cm^2 for the solder joint in this study is about 20°C, because the IMC growth is both thermally activated and electrically accelerated. For comparison, the anode and cathode IMC growth should be compared with isothermal aging at around 170°C. The IMC thick as a function of aging time and temperature is expressed empirically as

$$x = x_0 + A_0 t^n \exp\left(\frac{-\Delta H}{RT}\right) \quad (1)$$

where x is the IMC layer thickness at time t, x_o is the IMC layer thickness in the as-soldered condition, A_0 is the growth constant, and n is the time exponent. By conducting an isothermal aging test at various temperatures and times, the coefficients in Eq. 1 could be determined,[15] as for IMC growth at SAC387/ENIG:

$$x = (1.35 \pm 0.2) \times 10^{-6} + 4.92 t^{0.51 \pm 0.02} \exp[-(72.9 \pm 2.1) \times 10^3/RT] \quad (2)$$

where the apparent activation energy ΔH is determined as 73 kJ/mol and the time exponent is 0.51. The IMC growth at 170°C could be predicted by Eq. 2.

Understanding the joule heating effect, we are able to identify the scale of the EM effects on the

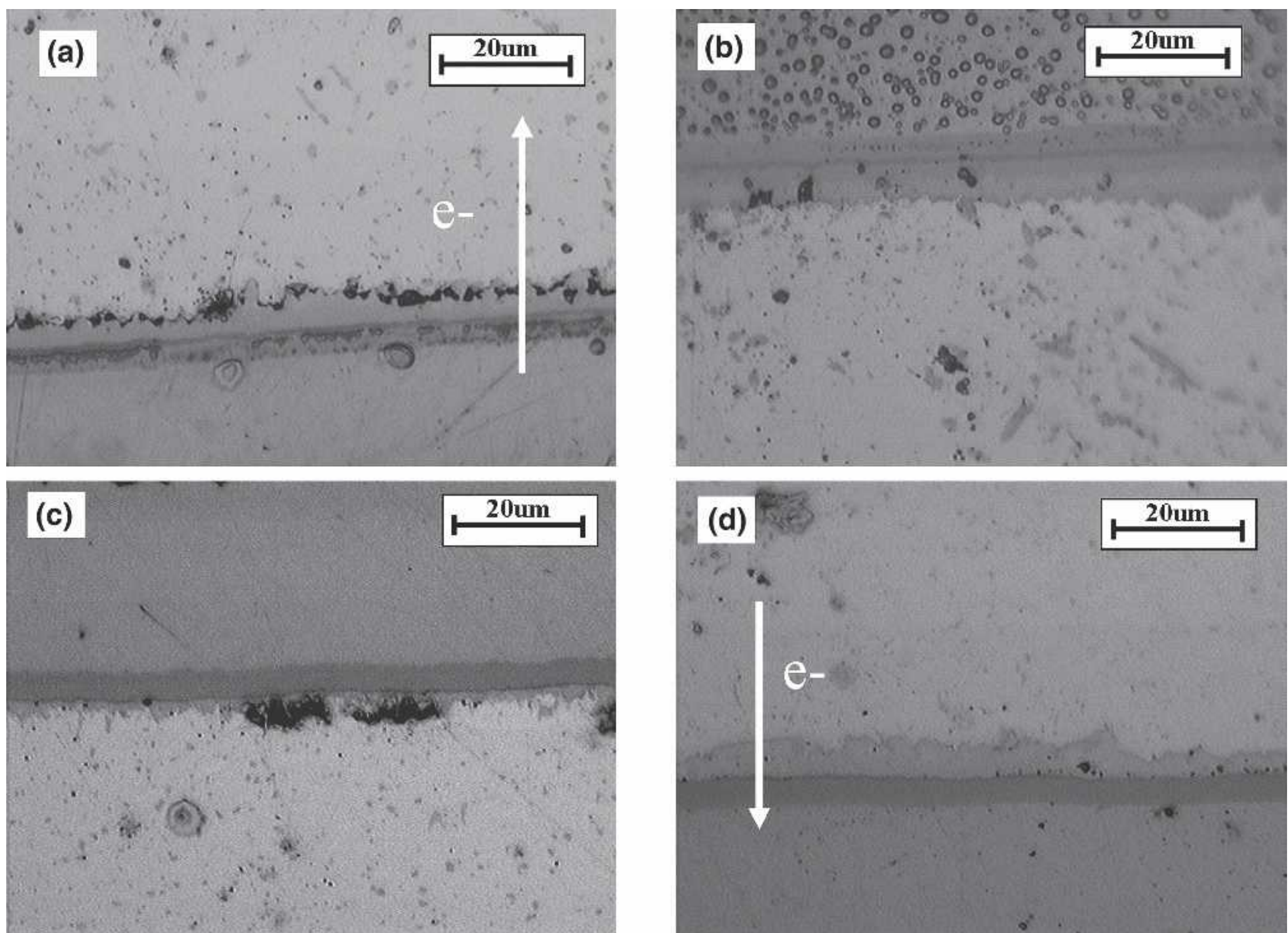

Fig. 10. IMC growth at Ni/SAC/ENIG; take Fig. 8 as reference. Solder ball a: (a) ENIG/SAC, cathode; (b) SAC/Ni anode, solder ball b; (c) Ni/SAC anode; and (d) SAC/Ni cathode.

intermetallic growth. In order to simplify the comparison between the samples with and without current, the IMC growth was assumed to obey the parabolic IMC growth rate, by which the time exponent is 0.5. Equation 1 could be simplified, and the IMC thickness, x, with or without current subject to the aging time can be described by

$$x = D\sqrt{t} + x_0 \quad (3)$$

$$D = A_0 \exp\left(\frac{-\Delta H}{RT}\right) \quad (4)$$

where D is defined as the diffusion coefficient (μm/sec$^{1/2}$), x_0 is the initial IMC thickness, and t is the aging time. By using Eq. 3 to curve fit the IMC thickness subject to the square root of time, as shown in Fig. 7, the diffusion coefficients can be obtained, as shown in Table I. The results for isothermal aging at 150°C and 170°C, D_{i150}, D_{i170}, cathode coefficient D_{c170}, and anode coefficient D_{a170}, are 0.0816, 0.3208, 0.472, and 0.1754, respectively, where the unit for time is hour. Thus, D_{i170}-D_{c170} is the dissolution coefficient caused by EM at 5,000 A/cm^2 at the cathode, while D_{a170}-D_{i170} is the elevator coefficient. The summary of their relationship is given in Table I. The diffusion constants here give the scale of the ion diffusion rate with and without the effect of EM.

Further IMC growth studies were observed on daisy-chained FPBGA solder joints with different surface finishes. The experimental setup was shown in Fig. 2. Five solder balls are selected in an FPBGA unit for passing current of 5,000 A/cm^2 at 125°C. After 10 days, the solder joint interfaces were cross-sectioned for observation.

Two types of surface finish, ENIG and Cu-OSP, are used in the board side. At the component side, the UBM is electrolytic Ni. Thus, four test conditions are included in the test samples. With respect to the direction of electron flow shown in Fig. 8, they are as follows. First is electrolytic Ni/SAC/Cu, where electron flux is from the Ni to Cu side. As shown in Fig. 9a and b, the growth of the Ni-Cu-Sn layer at the nickel side was slow, but IMC growth at the SAC/Cu side was slightly higher than isothermal aging. Second is Cu/SAC/electrolytic Ni, where electron flux is from Cu to Ni, as shown in Fig. 9c and d; some Cu_6Sn_5 particle IMCs were detected at the anode electrolytic Ni/SAC interface. This may indicate the migration of Cu from solder to the Ni/SAC interface. Third is ENIG/SAC/Ni, with electron flux from ENIG to electrolytic Ni, as shown in Fig. 10a and b; a void can be seen near the IMC/SAC interface at the cathode ENIG/SAC side. Fourth is Ni/SAC/ENIG, with electron flux from electrolytic Ni to ENIG, as shown in Fig. 10c and d. Voids were formed at the cathode Ni/SAC side, but not as significantly as in the case in Fig. 10c.

When comparing Fig. 9a and c, both of them are cathode, and the metallic substrates are electroless Ni (ENIG surface finish, gold layer already disappeared during soldering reflow) and electrolytic Ni, respectively. It seems that IMC growth for SAC/electrolytic Ni is faster than electroless Ni. For anode IMC growth shown in Fig. 9b and d, again, IMC growth for SAC/electrolytic Ni is faster than electroless Ni, because electroless Ni is a phosphorus containing layer, which eliminates the IMC growth rate.

The EM Effect on IMC Composition

EDX line scan composition analysis was conducted from the cathode to the anode (See Fig. 11). The distribution and concentration of Cu, Ni, and Sn are determined by their energy-dispersive peaks Cu K_α, Ni K_α, and Sn L_α, respectively. The intensity of secondary electrons is also shown in the figure. The local composition analyses on the anode and cathode within a distance of about 15 μm are shown in Fig. 12. Although the EDX line scan cannot provide quantitative data, it is useful in comparing the difference between the anode and cathode.

The actual compositions in the IMCs for different solder joints after EM exposure for 10 days are listed in Table II. Sample 1 is for the ENIG/SAC/ENIG single ball solder joint and the following are for the FPBGA specimens. From the table, it can be seen

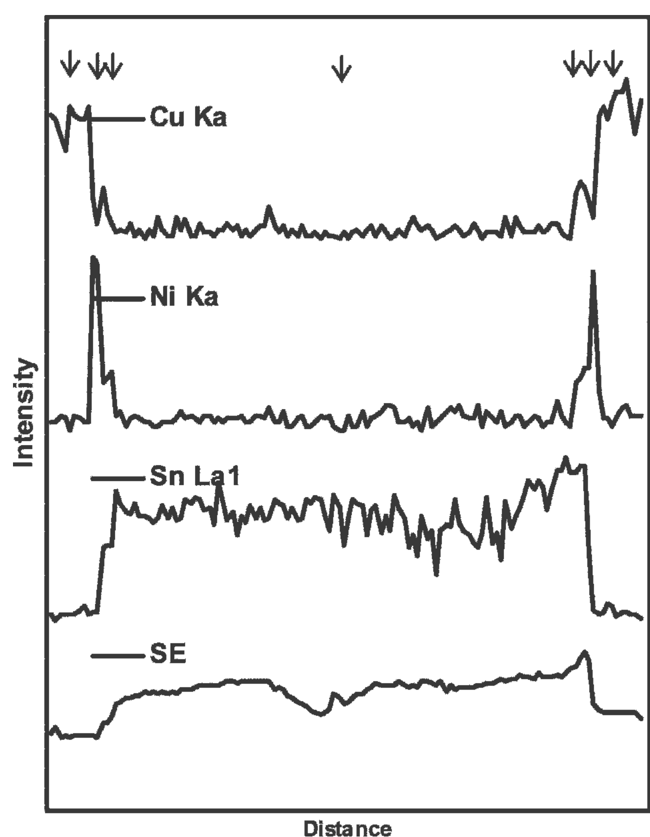

Fig. 11. EDX line scan to determine the distribution Cu, Ni, and Sn species from cathode (left) to anode (right) for the ENIG/SAC/ENIG single ball solder joint. For the arrows from left to right, (1) Cu, (2) Ni layer, (3) cathode IMC, (4) solder, (5) anode IMC, (6) Ni layer, and (7) Cu.

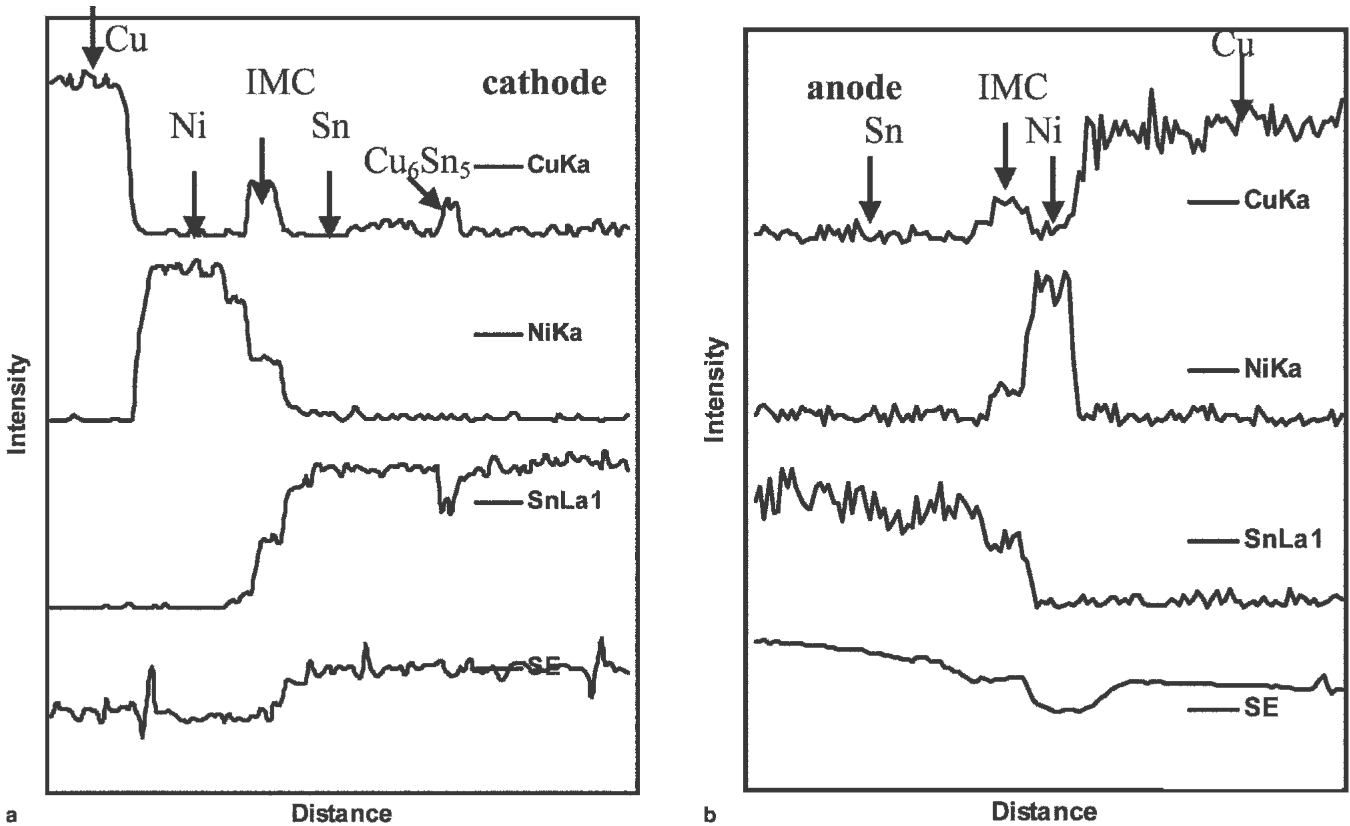

Fig. 12. EDX line scan to determine the local distribution Cu, Ni, and Sn species near the (a) cathode and (b) anode. It can be seen that more Ni layer is consumed at the anode side as more NiCuSn is formed.

that the species in IMCs are related to the local environment, i.e., solder composition and the corresponding metallization. However, long distance atomic electromigration seems to affect the IMC composition as well. For example, in sample 2, Ni atoms were detected in the IMC at the anode SAC/Cu interface in the electrolytic Ni/SAC/Cu solder joint. The Ni atoms could only be from electrolytic Ni at the cathode side; for comparison, the long distance Ni migration was not found at the SAC/Cu interface in an isothermally annealed specimen. If the electron flux is changed to the reverse direction from Cu to SAC to Ni, as for sample 3, the IMC at the cathode Cu/SAC is binary Cu_6Sn_5; Ni was not detected in the IMC. The nickel atomic diffusion driven by EM in this study is of interest because the existence of Ni atoms may affect the mechanical properties of the IMC layer. For other solder joint–like Ni/SAC/Ni, it is anticipated that the Ni atoms also diffuse in the entire solder along the electron flux, although it could not be proven by EDX analysis.

How the change of composition will affect the Young's modulus and hardness of IMCs was studied by nanoindentation. Planar IMC surface nanoindentation CSM was conducted. The solder joints were selectively deep etched to remove the Sn phase; the IMC layer was exposed for investigation. The reason of using planar IMC surface nanoindentation was reported in our earlier study.[11] The IMC layer of the actual solder joint is too thin (2–5 μm)

Table II. Comparison of IMC Composition at the Anode and Cathode for SAC with Different Metallization, Electron Flux is from the Left to Solder and Then to the Second Layer (Ni: Electroplated Ni)

No.	Solder Joint	Cathode IMC	Anode IMC
1	ENIG/SAC/ENIG	Ni, Cu, Sn (P)	Ni, Cu, Sn (P)
2	Ni/SAC/Cu	Ni, Cu, Sn	Ni, Cu, Sn
3	Cu/SAC/Ni	Cu, Sn	Ni, Cu, Sn
4	Ni/SAC/ENIG	Ni, Cu, Sn	Ni, Cu, Sn (P)
5	ENIG/SAC/Ni	Ni, Cu, Sn (P)	Ni, Cu, Sn

for the nanoindentation measurement from the cross-sectioned surface. As the IMCs at the interface tend to form a layer at the anode or the cathode during EM, it becomes very convenient to measure the Young's modulus and hardness from the planar IMC surface. For tests on the planar IMC surface, a test array 5 × 5 with a distance of 30 μm between every two indentations was conducted. To confirm a test was performed on the IMC, not the Cu or Ni layer, analyses of the load-displacement curve and modulus-displacement curve are necessary. Indentation measurements were conducted on interested IMC surfaces after completion of EM exposure for 10 days. The results of the modulus and hardness for the IMC and corresponding solder joint are listed in Table III. Figure 13 shows the

representative test curves for Cu_6Sn_5 at cathode Cu/SAC/electrolytic Ni (electron flux from Cu to Ni) and NiCuSn at anode Ni/SAC/Cu (electron flux from Cu to Ni). Figure 13a is the load-displacement curves. The corresponding Young's modulus and hardness, as a function of depth, are shown in Fig. 13b and c. Considering the polished IMC layer thickness is only several microns, the average modulus and hardness are taken from a low depth from 100 nm to 300 nm. As shown in Fig. 13b, the value of the modulus becomes "stable" after 50–100 nm, and it is independent of the depth into the surface. Because some parts of the IMC surface are still rough after a slight polish, the indents were checked by SEM and only those indents falling in the flat area are considered as accurate measurements. The Poisson's ratio of all the phases was approximated as 0.3 when calculating the true Young's modulus.

A summary of the Young's modulus for samples 1–5 is given in Table III. For specimen 1, the exact composition was measured by EPMA. From the concentration of Cu, we see that the Cu in the IMC at the anode is higher than that at the cathode. The modulus of the anode IMC, $(Cu_{0.73}Ni_{0.27})_6Sn_5$ for sample 1, is around 175 GPa, which is much higher than Cu_6Sn_5 (100 GPa), although they have the same crystal. On the cathode side, the crystal structure is also different; it is mainly $(Ni_{1-x}Cu_x)_3Sn_4$ with a modulus of 141 GPa. For sample 2, the formation of the NiCuSn ternary IMC rather than Cu_6Sn_5 produces a high Young's modulus of 161 GPa. In contrast, the cathode IMC at sample 3 is Cu_6Sn_5, the Young's modulus is 97.2 GPa, and the anode IMC is 176 GPa. The asymmetry of the mechanical properties again confirmed that the long distance atomic diffusion affected the composition. Our previous work[11] reported IMC growth and the change of modulus during isothermal aging. The Young's modulus and hardness for binary IMCs such as Cu_6Sn_5 and Ni_3Sn_4 are normally kept constant with thermal aging. However, for ternary IMCs such as NiCuSn, the crystal structure and thus the mechanical properties are sensitive with the ratio of Ni and Cu. More Ni will form $(Ni_{1-x}Cu_x)_3Sn_4$, while more Cu will form $(Cu_{1-x}Ni_x)_6Sn_5$. The latter one showed a high Young's modulus.

Table III. Young's Modulus of IMCs after EM Exposure for Different Solder Joints after Completion of the Test

No.	Solder Joint	Cathode IMC/Modulus (GPa)	Anode IMC/Modulus (GPa)
1*	ENIG/SAC/ENIG	$(Ni_{0.57}Cu_{0.43})_3Sn_4$/141	$(Cu_{0.73}Ni_{0.27})_6Sn_5$/175
2	Ni/SAC/Cu	NiCuSn/138	NiCuSn/161
3	Cu/SAC/Ni	Cu_6Sn_5/97.2	NiCuSn/176
4	Ni/SAC/ENIG	NiCuSn/140	NiCuSn/160
5	ENIG/SAC/Ni	Ni, Cu, Sn(P)/X	NiCuSn/X

*Measured by EPMA.

CONCLUSIONS

The EM has a significant impact on the IMC layer growth, both in growth rate and composition. The Joule heating effect can cause a fast IMC growth rate at both the anode and the cathode. The revolution of IMC composition leads to the change of mechanical properties. The Young's modulus and hardness measured by nanoindentation CSM showed different values on the anode and the cathode; e.g., the Young's modulus for the IMC at anode SAC/Ni side is approximately 180–190 GPa, while the value at the cathode Ni/SAC side is only 130–140 GPa. The EDX line scan analysis from the cathode to the anode detected the long-range Cu and Ni diffusion driven by EM and the effect on IMC composition. The EPMA measurement on the Ni/SAC/Ni specimen confirmed the polarized Ni and Cu distribution in the cathode and anode IMCs; the corresponding crystal structures were $(Ni_{0.57}Cu_{0.43})_3Sn_4$ and $(Cu_{0.73}Ni_{0.27})_6Sn_5$, respectively. The effect of polarized IMC mechanical properties on solder joint reliability requires further study.

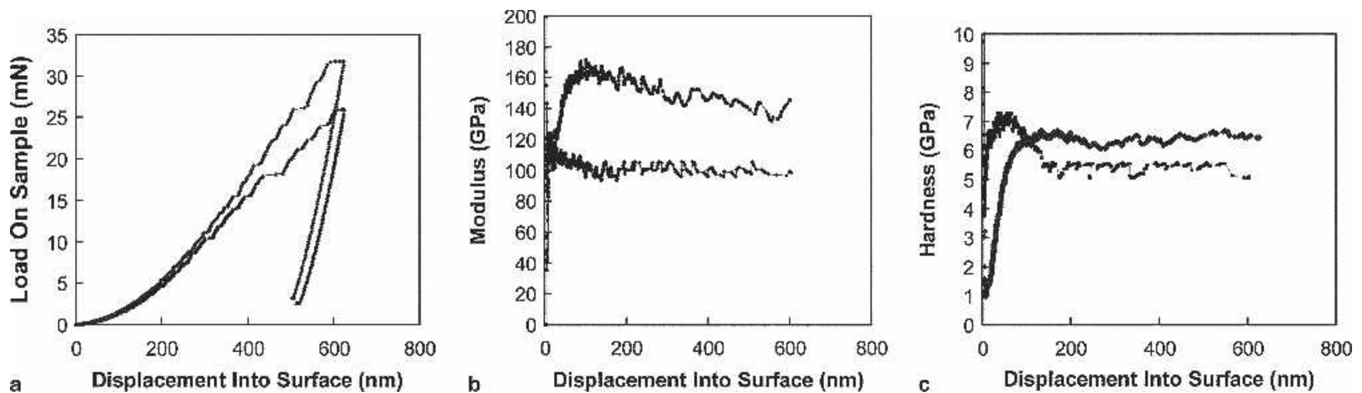

Fig. 13. Representative load, mudulus, and hardness versus displacement curves for interfacial IMCs: (1) load-displacement, (2) modulus-displacement, and (3) hardness-displacement. For each figure, the higher value curve is for NiCuSn in sample 2 and the lower value is for Cu_6Sn_5 in sample 3.

REFERENCES

1. M.R. Harrison, J.H. Vincent, and A.A.H. Steen, *Solder. Surf. Mt. Technol.* 13, 21 (2001).
2. E. Bradley, *Electron. Comp. Technol. Conf.* (New Orleans, LA: IEEE 2003), pp. 41–45.
3. A. Christou, *Electromigration and Electronic Device Degradation* (New York: Wiley-Interscience Publication, 1993), pp. 105–138.
4. D.G. Pierce and P.G. Brusius, *Microelectron. Reliab.* 37, 1053 (1997).
5. K.N. Tu, *J. Appl. Phys.* 94, 5451 (2003).
6. G.A. Rinne, *Electron. Packaging Technol. Conf.* (Piscataway, NJ: IEEE, 2003), pp. 72–76.
7. M. Tammaro, *J. Appl. Phys.* 86, 3612 (1999).
8. I.A. Blech, *Appl. Phys. Lett.* 29, 131 (1976).
9. K. Zeng and K.N. Tu, *Mater. Sci. Eng. R.* 38, 55 (2002).
10. C.M. Chen and S.W. Chen, *Acta Mater.* 50, 2461 (2002).
11. L.H. Xu and J.H.L. Pang, *Thin Solid Films* 504, 362 (2006).
12. J.H.L. Pang, L.H. Xu, X.Q. Shi, W. Zhou, and S.L. Ngoh, *J. Electron. Mater.* 33, 1219 (2004).
13. W.C. Oliver and G.M. Pharr, *J. Mater. Res.* 7, 1564 (1992).
14. X.D. Li and B. Bhushan, *Mater. Charact.* 48, 11 (2002).
15. L.H. Xu, J.H.L. Pang, K.H. Prakash, and T.H. Low, *IEEE Trans. Compon. Packaging Technol.* 28, 408 (2005).